01 Aug 2003

Modeling of Short-Gap ESD under Consideration of Different Discharge Mechanisms

S. Bonisch

Wilifried Kalkner

David Pommerenke

Missouri University of Science and Technology, davidjp@mst.edu

Modeling of Short-Gap ESD Under Consideration of Different Discharge Mechanisms

Sven Bönisch, Wilfried Kalkner, and David Pommerenke, *Member, IEEE*

***Abstract*—Simulation of short gap electrostatic discharge (ESD) in air needs to consider two processes: a surface process and an avalanche process. Two models, a phenomenological approach and a physical approach, considering both discharge processes are proposed for the simulation of short-gap ESD. A new mathematical derivation for the modeling of the surface process is discussed in detail. A new technique to combine surface and avalanche process models is described. Measured and simulated data based on short-gap ESD are provided and compared. Advantages and drawbacks of the proposed models are discussed. Attained results should help to optimize ESD testing.**

***Index Terms*—Arc model, electrode material, short-gap electrostatic discharge (ESD), surface process.**

I. Introduction

SHORT-GAP electrostatic discharge (ESD) development depends on two different processes: a surface process and an avalanche process. Both processes contribute to ionization and arc development in air. However, at the present time a model taking both processes into account does not exist. While simulation of the avalanche process is well known [16]–[19], [22], [23], [28] and surface processes in pulsed vacuum discharges have been extensively studied [6]–[15], neither the surface process in gas-filled gaps nor the combination of surface and avalanche processes have been modeled before.

This investigation provides models for the description of the electrical parameters of an arc discharge in gas, based on measurement data of short-gap ESD. Two models are proposed for modeling of short-gap ESD: a simple phenomenological model and a more complicated physical model. A new technique to combine surface and avalanche modeling is introduced. A mathematical derivation of the surface process modeling and its physical background are given. The advantages and drawbacks of the proposed models compared to measurement data on short-gap ESD are discussed in detail. The attained results should help to optimize ESD testing.

II. Measurement and Simulation Setup

A. Measurement Setup

The measurement setup used for investigating ESD current rise [1] is shown in Fig. 1. It consists of a pulse generator, a planar gap in the center conductor of a coaxial transmission line and a 50-Ω load. The current is measured using a sampling scope with 20-GHz bandwidth. The coaxial spark gap is constructed of two brass fittings (Ø 9.5 mm). For achieving a uniform field, the inner conductor ends (Ø 4.1 mm) are machined to form a plane semisphere arrangement. The surface roughness (<2 μm after 10–100 discharges) is more than 1 order below the gap distance (60 μm). This has been shown using scanning electron microscope (SEM) techniques, and also reported by Nitta *et al.* [31]. Three parameter ranges for short-gap ESD at metallic electrode surfaces involving different surface and avalanche processes are given in Table I.

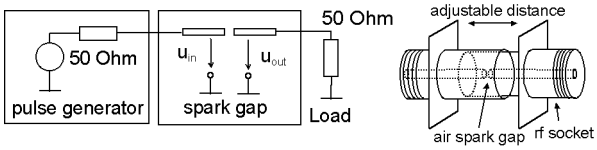

Fig. 1. Measurement setup and coaxial spark gap used for ESD current measurement [1].

TABLE I
Parameter Ranges for Short Gap ESD at Metallic Electrode Surface [1]

Parameter range	1	2	3
Risetime (ps)	<40	300-600	<350
Current rise shape	No Step	Step	No Step
Gap distance (μm)	<10	20-80	80-100
Breakdown voltage (V)	<700	700-2000	>1500
Field strength (kV/mm)	>50-100	25-75	<8-35
Cathode influence	Yes	Yes	No
Anode influence	Yes	No	No
Gas pressure influence	No	Yes	Yes
Process	Surface	Surface & Avalanche	Avalanche

B. Simulation Setup

A simplified equivalent circuit as shown in Fig. 2 has been derived for simulating the discharge current $i_{\mathrm{arc}}(t)$. Two equivalent, time-dependent arc resistors model the arc channel. Each of them includes externally measurable effects of discharge processes into the model. For the surface process $R_{\mathrm{surf}}(t)$ has been included, while $R_{\mathrm{av}}(t)$ is used to calculate the effect of the avalanche process. After that, the currents $(i_{\mathrm{surf}}(t), i_{\mathrm{av}}(t))$ are calculated using the arc voltage $U_{\mathrm{arc}}(t)$ and the corresponding equivalent arc resistance. The resistance R is the sum of all resistances external to the spark gap. The source voltage U_s is assumed to be constant during the time of discharge development as the rise time of the pulse generator (≈ 5 ns) is about 1 order

Manuscript received August 28, 2002; revised March 11, 2003. This work was supported by the Deutsche Forschungsgemeinschaft (DFG).

S. Bönisch and W. Kalkner are with High Voltage Engineering, Technical University of Berlin, D-10587 Berlin, Germany (e-mail: boenisch@ihs.ee.tu-berlin.de; kalkner@ihs.ee.tu-berlin.de).

D. Pommerenke is with the Electromagnetic Compatibility Laboratory, University of Missouri-Rolla, Rolla, MO 65409-0040 USA (e-mail: pommerenke@ece.umr.edu).

Digital Object Identifier 10.1109/TPS.2003.815823

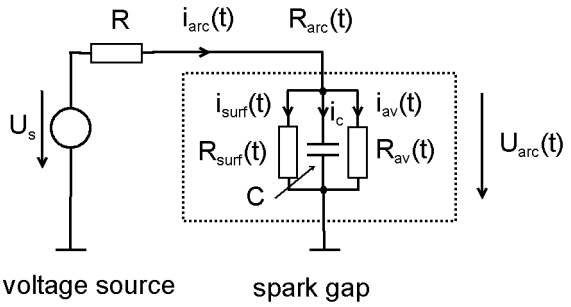

Fig. 2. Equivalent circuit for the discharge current simulation.

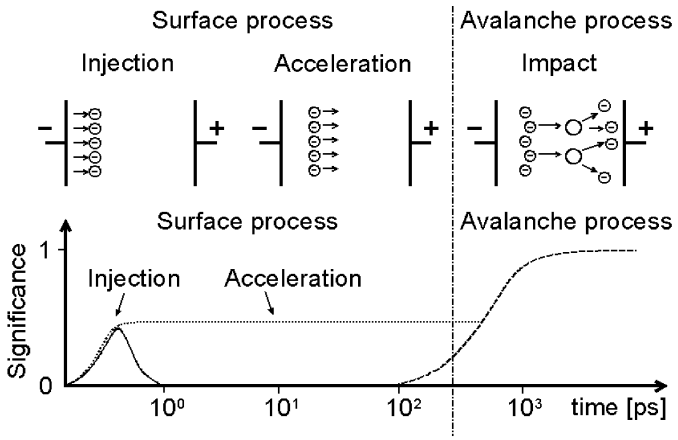

Fig. 3. Time-dependent process significance.

longer than the rise time of the discharge development at the gap ($<$600 ps) [1].

C. Process Separation Method

The surface process and the avalanche process are assumed to be separable in time (Fig. 3). In our case, the surface processes summarizes the injection and acceleration of initial charge carriers (electrons), while the avalanche process describes only impact and ionization processes.

It has been experimentally demonstrated, that the surface process develops independent of the avalanche process [1]. This has been done by comparison of the current rise shape at different gas pressures. The risetime of the current related to the surface process is independent of the gas pressure, while the risetime of the current related to the avalanche process varies with the gas pressure (Fig. 3).

The surface process, however, influences the avalanche process, namely the steepness of the related current rise, by injection of charge carriers into the gap (chapter IV). However, during the time of the charge carrier injection (which is extremely small $<$40 ps by measurement, approximately 1–10 ps by theoretical considerations), there is no avalanche (charge-carrier multiplication) inside the gas because the electron energy is below the ionization energy. The charge-carrier injection has ended a long time before the avalanche process becomes significant. Due to the nature of the charge carrier multiplication by electron impact, the current risetime for the avalanche process ($>$300 ps) is much longer than the current risetime for the surface process ($<$40 ps, difference 1 or 2 orders in time). This time difference is mainly determined by the acceleration of the electrons to an energy sufficient to cause gas ionization. Even though the surface process injects charge carriers into the volume (gas), which are sufficient to influence the avalanche process later in time, during the injection phase they do not influence. This special behavior has been understood and modeled by keeping the equivalent arc resistance of the surface process constant after the finish of the injection process. This unconventional approach may be a subject to discussion of applicability, but the attained results show a good agreement with measured data.

Thus, both processes are assumed to be independent and separable in time and it is possible to combine the equivalent arc resistances of the surface process and the avalanche process to get a consistent description of the discharge development.

III. Modeling of Short-Gap ESD

Modeling of ESD in gaseous media is well known [4], [5], [16]–[19]. However, the modeling of short-gap ESD must consider two independent processes: a surface process and an avalanche process. Both processes contribute to the arc channel development [1].

Our first approach (phenomenological model) is more empirical, it describes voltage and current at the gap avoiding detailed analysis of the physical processes. A newly developed mathematical model has been used to simulate the surface process. Our second approach (physical model) applies a model that is originated from research on vacuum discharges in combination with a refined avalanche model. Both models have been designed and tested for the following conditions.

- Air gap distance: 6–140 μm.
- Arc channel diameter: 200–400 μm.
- Pulsed voltage source: 0–2000 V.
- Risetime: 5 ns.
- Overvoltage factor: 2–3.
- Electrode diameter: 4.1 mm.
- Uniform field strength: 10–120 kV/mm.
- Air pressure: 2.7–101 kPa.

A. Phenomenological Model

1) Avalanche Process: The phenomenological model uses the "Toepler Law" [16], [17] for modeling the avalanche. Detailed mathematical derivation can be found at Pommerenke [4] and Küchler [5]. The "Toepler Law" assumes charge carrier generation via impact ionization. Only fast charge carriers (electrons) are taken into account. The number of charge carriers generated per unit length is described by the ionization coefficient α. Recombination and field strength dependency of the ionization coefficient are neglected. The arc channel is in thermal equilibrium. The charge carrier density is constant over the radius of the arc channel. The calculation of the equivalent, time dependent arc resistance $R_{\rm av}(t)$ as a consequence of charge carrier accumulation via electron impact is given by (1). The integral describes the complete charge, which has flown through the channel up to the time t.

$$R_{\rm av}(t) = \frac{a_T \cdot d}{\int_0^t i_{\rm av}(\xi) d\xi} \tag{1}$$

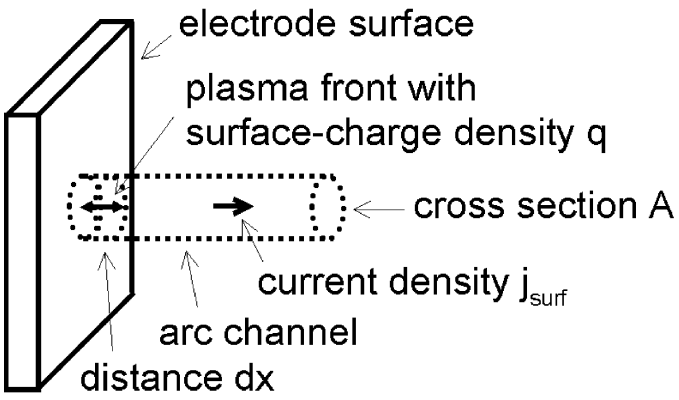

Fig. 4. Arc channel at electrode surface.

where

a_T "Toepler Arc Constant" ($\approx 5 * 10^{-3}$ Vs/m for air at normal pressure);
d electrode distance = arc channel length (m);
i_{av} arc current due to the avalanche process (A).

2) Surface Process: For the modeling of the surface process the extraction of charge carriers from electrode surface into the volume (gas fill) is of particular interest. The calculation of the current $i_{\text{surf}}(t)$ is based on charges that have been extracted from the electrode surface. These charges form the surface-charge density q (i.e., a thin layer of electrons at the plasma front) and the current density j_{surf} inside the arc channel. The distance between the electrode surface and the plasma front is given by dx. The type, drift velocity, and acceleration of the charge carriers involved is not further analyzed. The arc channel may be infinitely long. Impact and recombination processes have been neglected. Fig. 4 shows a schematic drawing of the interface between the electrode surface and the gas filled space.

The current density inside the channel can be described as an (unknown) charge multiplied by the time derivative of the charge carrier density (particles per area) at the plasma front

$$j_{\text{surf}} = b \cdot e \cdot \frac{dn}{dt}. \tag{2}$$

The integration over time leads to the surface-charge carrier density at the (moving) plasma front. The surface-charge carrier density describes the carrier density in a thin layer of charges (at the plasma front) injected by the surface process and moving in the volume (gas) or arc channel up to a time where the carrier energy is sufficient to start the avalanche process. The phrase "surface-charge" should indicate that the carriers are concentrated in a very thin layer, the plasma front, so that we can assume to solve a two-dimensional (2-D) problem. Of course, this layer is moving in three-dimensional (3-D) space, but due to the very fast carrier injection the spatial dimension of this layer in the x-axis is negligible

$$n = \frac{1}{b \cdot e \cdot A} \cdot \int_0^t i_{\text{surf}}(\xi) d\xi \tag{3}$$

where

n surface-charge carrier density at the plasma front, particles per area (m^{-2});
A arc channel cross section (m^2);
b number of elementary charges per charge carrier (unitless);
e elementary charge $(\text{A}*s)$;
i_{surf} arc current supplied by the surface process (A);
t time (s);
ξ integration variable.

The derivative of the surface-charge carrier density with respect to dx may be described as the product of a "charge carrier extraction coefficient" and the surface-charge carrier density at the plasma front as follows:

$$\frac{dn}{dx} = \alpha_M \cdot n \tag{4}$$

where α_M is the "charge carrier extraction coefficient" (m^{-1}).The drift velocity of the charge carriers due to the applied electric field can be calculated by

$$v = \mu_M \cdot E = \frac{dx}{dt} \tag{5}$$

where

v drift velocity of the charge carriers $(m*s^{-1})$;
μ_M charge carrier mobility ($\text{m}^2*\text{V}^{-1}*\text{s}^{-1}$);
E field strength ($\text{V}*\text{m}^{-1}$).

This leads to

$$\frac{dn}{dt} = \alpha_M \cdot n \cdot v. \tag{6}$$

Substituting into (2)

$$\frac{j_{\text{surf}}}{b \cdot e} = \alpha_M \cdot n \cdot v. \tag{7}$$

Using (3) the arc current as a function of time can be described as

$$i_{\text{surf}}(t) = \alpha_M \cdot v \cdot \int_0^t i_{\text{surf}}(\xi) d\xi. \tag{8}$$

The substitution of drift velocity by carrier mobility and field strength gives

$$i_{\text{surf}}(t) = \alpha_M \cdot \mu_M \cdot E \cdot \int_0^t i_{\text{surf}}(\xi) d\xi. \tag{9}$$

Finally, a new constant, the "surface process constant," is defined which describes the behavior of the charge carriers supplied by the surface process as

$$a_M = \frac{1}{\alpha_M \cdot \mu_M} \tag{10}$$

where

a_{M} "surface process constant" ($\text{V}*\text{s}*\text{m}^{-1}$);
α_{M} "charge carrier extraction coefficient" (m^{-1});
μ_{M} charge carrier mobility for the surface process ($\text{m}^2*\text{V}^{-1}*\text{s}^{-1}$).

The equivalent arc channel resistance can be calculated using

$$E = \frac{U}{d} \tag{11}$$

where U is the arc voltage (V) and d is the gap distance = arc length (m), which gives

$$R_{\mathrm{surf}}(t) = \frac{a_M \cdot d}{\int_0^t i_{\mathrm{surf}}(\xi) d\xi}. \tag{12}$$

Fortunately, (12) has the same structure as (1), but with a different constant. The value of the "surface process constant" a_{M} is derived empirically to fit the measured data. It is strongly dependent on the electrode material, for brass it has a value of about $4 * 10^{-4}$ Vs/m.

3) Combination of Both Processes: The time that the two processes need for the development differs by about one order of magnitude. This is the reason to assume that they can be modeled independently. First, the contribution of each process is calculated, neglecting the other one. Then, both are combined (13) using the parallel circuit approach shown in Fig. 2

$$R_{\mathrm{arc}}(t) = \frac{R_{\mathrm{surf}}(t) \cdot R_{\mathrm{av}}(t)}{R_{\mathrm{surf}}(t) + R_{\mathrm{av}}(t)}. \tag{13}$$

There is a limit to which the surface process can contribute charge carriers: For field strengths below a threshold, the surface process cannot supply any charge carriers, the equivalent arc resistance of that process remains constant. We name this value the "surface process threshold field strength." The threshold field strength has been considered introducing a probability function which describes the fading of the surface process

$$W(E) = \frac{\left(\frac{E}{E_T}\right)^m}{1 + \left(\frac{E}{E_T}\right)^m} \qquad m > 10 \tag{14}$$

where

$W(E)$	probability of charge carrier extraction (unitless);
E_T	"surface process threshold field strength" (V$*$m^{-1});
E	field strength (V$*$m^{-1});
m	order of polynomial function (unitless).

B. Physical Model

1) Avalanche Process: The avalanche model used here has been derived from the "Extended Toepler Law" [4]. It assumes charge carrier generation via impact ionization. Only fast charge carriers (electrons) are taken into account. The number of charge carriers generated per unit length is described by a field strength dependent ionization coefficient α. The charge carrier drift velocity v is also assumed to be field strength dependent. The arc channel is in thermal equilibrium and the charge carrier density is constant over the radius of the arc channel. At short-gap distances, the electrode capacitance displacement current (i_{C}) needs to be taken into account. The displacement current cannot be measured at the terminals of the gap, but leads to faster arc channel development by supplying energy to the charge carriers due to the discharge of the gap capacitance C. It is described by the first term of the sum in (15). Furthermore, the avalanche may be start with an initial number of charge carriers (N_0). The avalanche process can be described by the following system of equations.

$$i_{\mathrm{av}}(t) = C \cdot \frac{dU_{\mathrm{arc}}(t)}{dt} + N_0 \cdot \frac{e \cdot v(t)}{d} \cdot \exp\left(\int_0^t \alpha(\xi) \cdot v(\xi)\, d\xi\right) \tag{15}$$

$$i_{\mathrm{av}}(t) = \frac{U_s - U_{\mathrm{arc}}(t)}{R} \tag{16}$$

where C is the gap capacitance (F) and N_0 is the initial number of charge carriers supplied by the surface process (unitless). The impact ionization coefficient α for air discharges has been investigated by Meek and Craggs [23] and Korolev and Mesyats [28]. It shows an exponential field strength dependency given by (17)

$$\frac{\alpha}{p} = A \cdot \exp\left(-\frac{B \cdot p}{E}\right) \tag{17}$$

where p is the gas pressure (torr).

Gas type dependent approximation coefficients for α in air at normal pressure [28] and approximations for different electrode materials developed in this work are given in Table II, the exponential dependency of α on the field strength can be seen in Fig. 5. For short-gap ESD, the ionization coefficient needs to be about 1 order less than known values to fit the measured data.

Korolev and Mesyats [28] provide also an approximation of the drift velocity of electrons in gaseous media at different pressures (18) which predicts the dependency on field strength and gas pressure (Fig. 6). The coefficient γ at high field strengths

TABLE II
APPROXIMATION COEFFICIENTS USED BY (17)

Approximation coefficient	A (Torr/m)	B (V*Torr/m)
Korolev et al. [28]	1.5*10^3	3.65*10^4
Brass electrode material	2*10^2	3.4*10^4
Aluminum electrode material	1.33*10^2	3.4*10^4
Steel electrode material	1.1*10^2	3.3*10^4

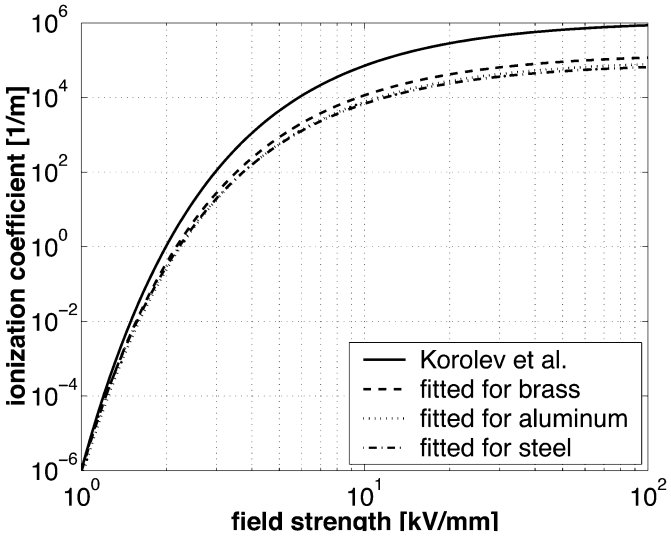

Fig. 5. Ionization coefficient α in air at normal pressure.

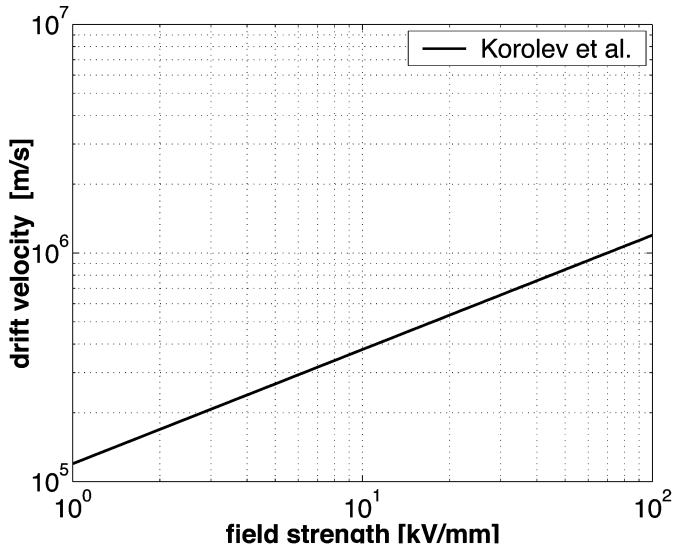

Fig. 6. Drift velocity v of electrons in air at normal pressure.

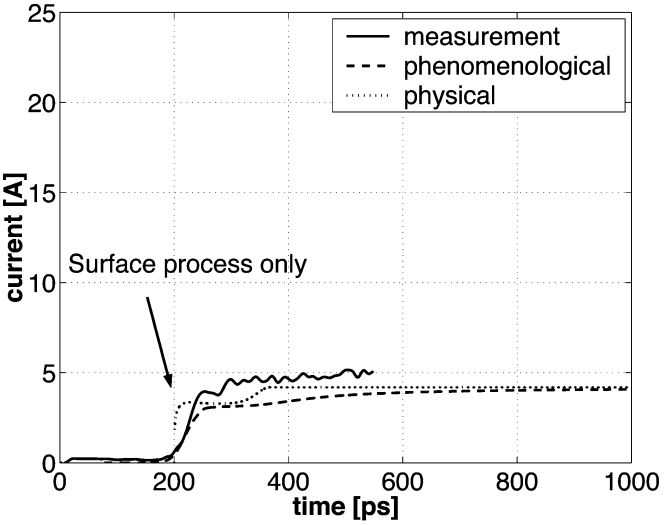

Fig. 7. Measurement and simulation of short-gap ESD arc current (electrode material brass, breakdown voltage 420 V, gap distance 10 μm, $a_{\mathrm{M}} = 4 * 10^{-4}$ Vs/m, $a_T = 8 * 10^{-4}$ Vs/m, $E_T = 12$ kV/mm, $\mathrm{K}(\alpha) = 0.8$).

has not been found to be consistent in literature but fit our measured data

$$v = C \cdot \left(\frac{E}{p}\right)^{\gamma}$$
$$C = 3.3 \cdot 10^{6} \frac{\mathrm{cm}^{3/2} \cdot \mathrm{torr}^{1/2}}{s \cdot \mathrm{V}^{1/2}}$$
$$\gamma = 0.5 \ (\text{for air}) \tag{18}$$

2) Surface Process: In [1], it was shown that the surface process in a short-gap ESD experiment is similar in nature to a pulsed vacuum discharge. This allows the utilization of a model that has been developed by Mesyats and Proskurovsky [27] for the computation of pulsed vacuum discharges. Following that model, a plasma front develops at cathode surface protrusions mainly due to resistive heating, melting and explosive particle emission [6]–[15]. The plasma front moves toward the anode causing a current at the gap terminals. According to [27], the current can be described by the following system of equations:

$$i_{\mathrm{surf}}(t) = \frac{4}{9} \cdot \varepsilon_0 \cdot \sqrt{\frac{2 \cdot e}{m_e}} \cdot \frac{S_n(t) \cdot U_{\mathrm{arc}}(t)^{3/2}}{(d - v(t) \cdot t)^2} \cdot K(\alpha(t)) \tag{19}$$

$$i_{\mathrm{surf}}(t) = \frac{U_s - U_{\mathrm{arc}}(t)}{R} \tag{20}$$

where

$K(\alpha)$ shielding coefficient of the plasma front (unitless);
m_{e} electron mass (kg);
S_{n} cross section of the plasma front (m^2).

The negative space-charge density of the plasma front reduces the field strength at the cathode surface, which can be empirically described by a shielding coefficient. Levintov [24] assumes for K(α) a constant value of 0.3–0.6 which corresponds to our measurement data. The cross section of the arc channel is the product of the number of plasma channels and the cross section of one channel. It is assumed that each surface protrusion is a source of one conical plasma channel. The number of protrusions has been investigated using SEM techniques [1]. For brass electrode surface, used in the experiments, the number of protrusions for an arc cross section of about 0.15 mm^2 has been estimated to $N_{\mathrm{prot}} = 14\,000$

$$S_n(t) = N_{\mathrm{Prot}} \cdot \frac{1}{2} \cdot \pi \cdot (v \cdot t)^2 \tag{21}$$

where N_{Prot} is the number of surface protrusions (unitless).

3) Combination of Both Processes: The combination has been done in a similar way as in the phenomenological model. First, the contribution of each process is calculated, neglecting the other one. Then, both are combined (13) using the parallel circuit approach shown in Fig. 2. The fading of the surface process is inherent in (19) by taking the shielding action of the plasma front [K(α)] into account.

In this model, the extremely fast surface process supplies an initial number of charge carriers N_0 to the avalanche process, which develops later in time. The number of initial charge carriers has been calculated from the current supplied by the surface process and one time step of the numerical simulation

$$N_0 = \frac{i_{\mathrm{surf}} \cdot dt}{e} \tag{22}$$

where dt is the time step of numerical simulation (s).

IV. Results and Discussion

All simulations have been done using numerical calculation under "MATLAB." The results for measured and simulated arc discharge current in different parameter ranges can be seen in Figs. 7–10. The starting arc resistance has been assumed to be 10 MΩ. The constants for the phenomenological model have been: $a_{\mathrm{M}} = 4 * 10^{-4}$ Vs/m and $a_T = 8 * 10^{-4}$ Vs/m. The order of the probability function W(E) has been set to $m = 30$. The match to the measured data has been achieved using a surface process threshold field strength for brass electrodes of about 12 kV/mm. Both models are able to reproduce the measured current in reasonable manner. The surface process constant for the phenomenological model (a_{M}) and the shielding coefficient

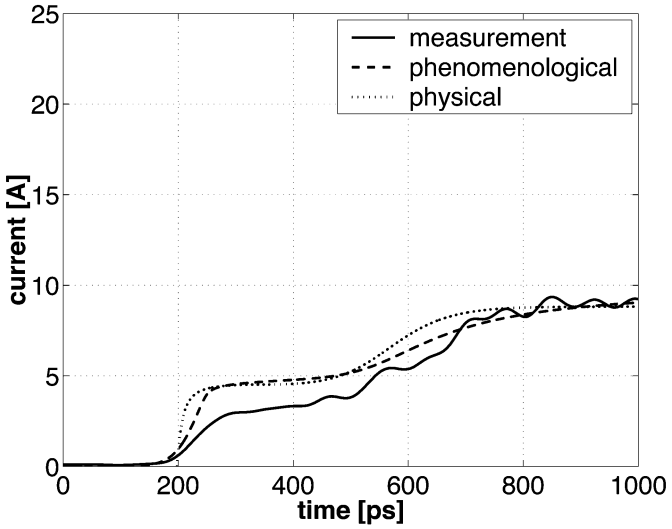

Fig. 8. Measurement and simulation of short-gap ESD arc current (electrode material brass, breakdown voltage 1000 V, gap distance 50 μm, $a_{\mathrm{M}} = 4 * 10^{-4}$ Vs/m, $a_T = 8 * 10^{-4}$ Vs/m, $E_T = 12$ kV/mm, $\mathrm{K}(\alpha) = 0.45$).

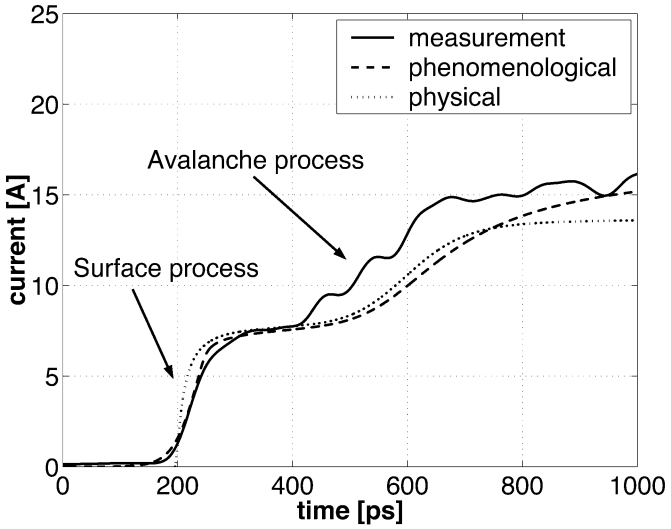

Fig. 10. Measurement and simulation of short-gap ESD arc current (electrode material brass, breakdown voltage 1700 V, gap distance 90 μm, $a_{\mathrm{M}} = 4 * 10^{-4}$ Vs/m, $a_T = 8 * 10^{-4}$ Vs/m, $E_T = 12$ kV/mm, and $\mathrm{K}(\alpha) = 0.45$).

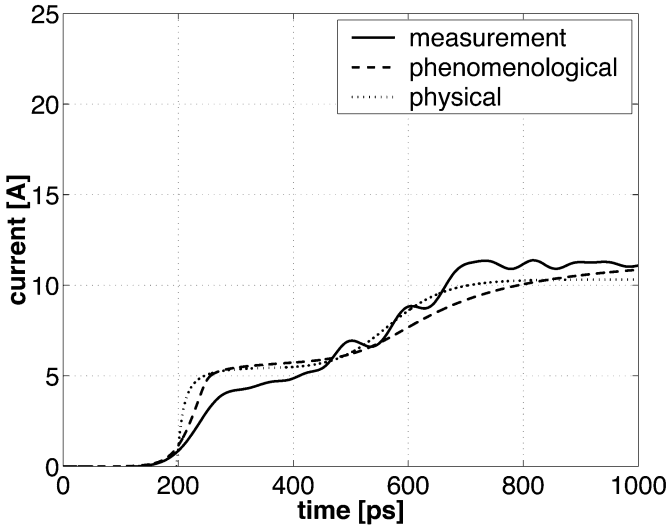

Fig. 9. Measurement and simulation of short-gap ESD arc current (electrode material brass, breakdown voltage 1200 V, gap distance 60 μm, $a_{\mathrm{M}} = 4 * 10^{-4}$ Vs/m, $a_T = 8 * 10^{-4}$ Vs/m, $E_T = 12$ kV/mm, and $\mathrm{K}(\alpha) = 0.45$).

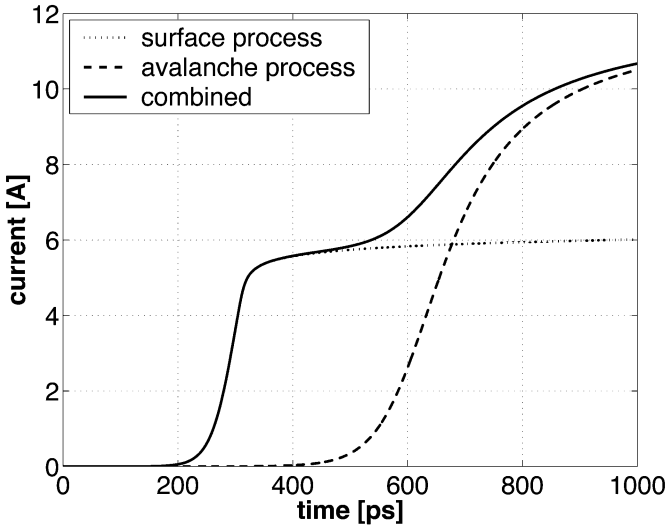

Fig. 11. Simulation of short-gap ESD arc current (electrode material brass, breakdown voltage 1200 V, gap distance 60 μm, phenomenological model, $a_{\mathrm{M}} = 4 * 10^{-4}$ Vs/m, $a_T = 8 * 10^{-4}$ Vs/m, and $E_T = 12$ kV/mm).

(K(α)) for the physical model need to be fitted to the measured data. The current risetime measurement is bandwidth limited by the measurement setup to about 40 ps. This may affect the surface constant a_{M} which may reflect more the measurement system bandwidth limit than the real risetime of the ESD current. The high gain supplied by α and an iterative loop process causes the simulation to become unstable under some conditions.

The phenomenological model shows for higher charge voltages lower maximum currents and lower di/dt than expected. Pommerenke [4] discussed the errors of the "Toepler Law" in detail. As the phenomenological model uses the same structure for the avalanche and the surface process, one might expect that the principle errors will affect both processes in a similar fashion.

The physical model has a more complicated structure. The shielding coefficient $\mathrm{K}(\alpha)$ needs to be tuned for different gap distances to fit the measured data. The surface process simulation by the physical model (Mesyats) describes the current risetime ($\approx$10 ps) quite well but has the major drawback that it cannot describe a time delay between application of voltage to the gap and current flow. Furthermore the "Extended Toepler Law," using known ionization coefficient α (Fig. 5) and an initial number of charge carriers supplied by the surface process, is not able to produce correct results. The ionization coefficient α needs to be about one order below known values to fit the measurement data.

Considering all this, the phenomenological model seems to be more suitable and accurate for short-gap ESD arc current simulation in different parameter ranges.

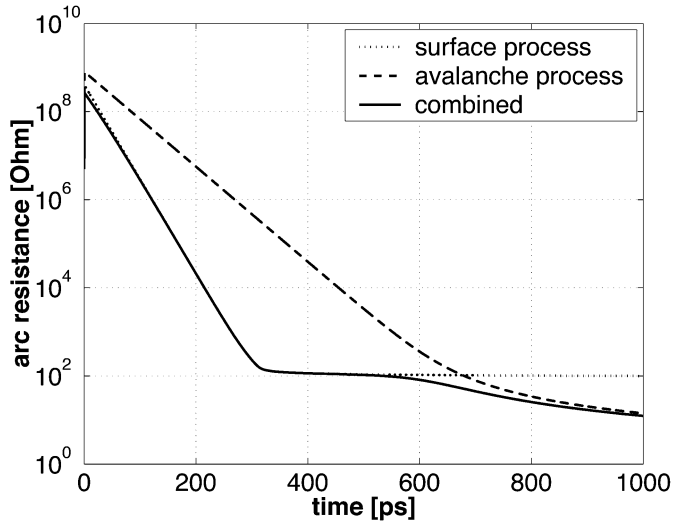

Fig. 12. Simulation of short-gap ESD arc resistance (electrode material brass, breakdown voltage 1200 V, gap distance 60 μm, phenomenological model, $a_{\mathrm{M}} = 4 * 10^{-4}$ Vs/m, $a_T = 8 * 10^{-4}$ Vs/m, and $E_T = 12$ kV/mm).

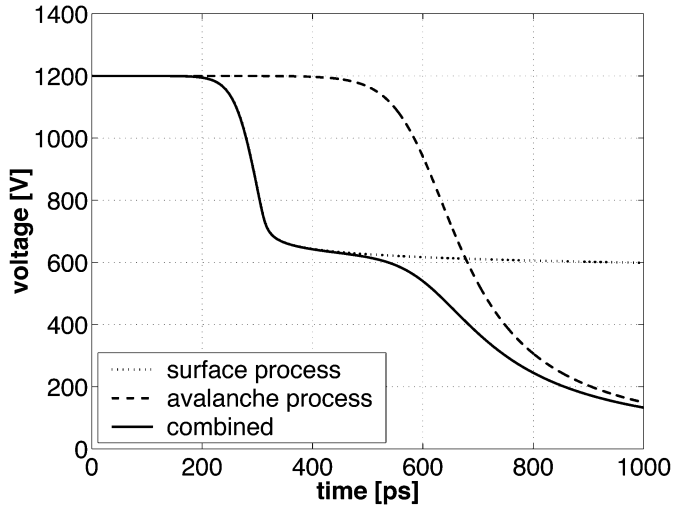

Fig. 13. Simulation of short-gap ESD arc voltage (electrode material brass, breakdown voltage 1200 V, gap distance 60 μm, phenomenological model, $a_{\mathrm{M}} = 4 * 10^{-4}$ Vs/m, $a_T = 8 * 10^{-4}$ Vs/m, and $E_T = 12$ kV/mm).

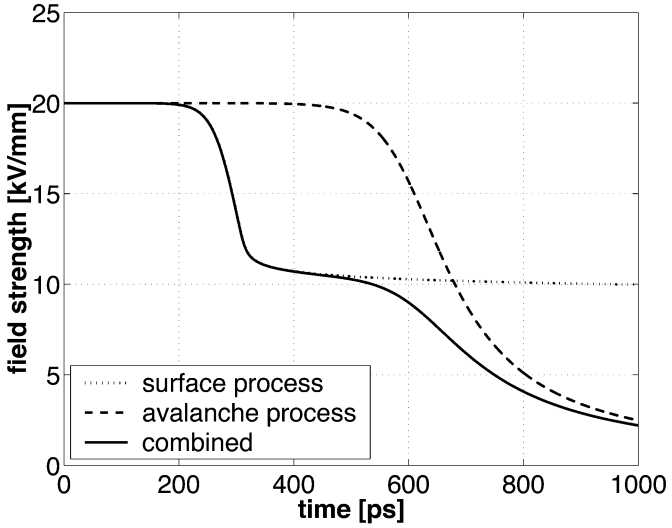

Fig. 14. Simulation of short-gap ESD field strength (electrode material brass, breakdown voltage 1200 V, gap distance 60 μm, phenomenological model $a_{\mathrm{M}} = 4 * 10^{-4}$ Vs/m, $a_T = 8 * 10^{-4}$ Vs/m, and $E_T = 32$ kV/mm).

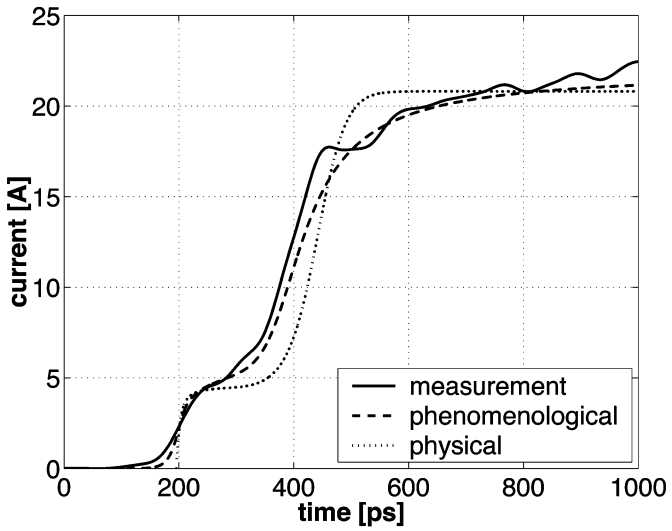

Fig. 15. Measurement and simulation of short-gap ESD arc current (electrode material aluminum, breakdown voltage 2200 V, gap distance 60 μm, $a_{\mathrm{M}} = 4 * 10^{-4}$ Vs/m, $a_T = 8 * 10^{-4}$ Vs/m, $E_T = 32$ kV/mm, and $\mathrm{K}(\alpha) = 0.2$).

Figs. 11–14 show the behavior of voltage, current, arc resistance, and field strength for the surface and the avalanche process of the phenomenological model in detail. The current (Fig. 11) rises due to the surface process in an extremely short time ($<$40 ps) from 0 up to 6 A. Below the surface process threshold field strength (12 kV/mm) the surface process is not able to produce charge carriers. Current, voltage and field strength at the terminals remain constant for about 200 ps. In parallel, an avalanche process starts to develop. At about 400 ps, the avalanche process is able to carry a current of $>$6 A. The current rises due to the avalanche process up to a value of 11 A, limited by the applied voltage and the source resistance R. The risetime of the surface process is at least one order below the risetime of the avalanche process. The logarithmic drop of the arc channel resistance is in good agreement with measured data on short-gap ESD. It shows an asymptotic behavior with a lower border at about 10 Ω, caused by an equilibrium of electrical input power and thermal as well as recombination losses.

Figs. 15 and 16 show the simulation of short-gap ESD arc current at different electrode materials. Table III shows the constants used for current simulation of ESD at different electrode materials. It can be clearly seen that the type of electrode material influences the surface process threshold field strength and the current supplied by the surface process. Thus, the number of initial charge carriers varies with the electrode material (Fig. 17). Materials having a lower melting point (brass) seem to supply a higher current and more charge carriers due to the surface process. This may be a reason for the risetime variation of the avalanche process with the electrode material. The aluminum surface builds up a high melting point oxide layer at the surface which acts as an additional insulation layer for field electron emission, reducing

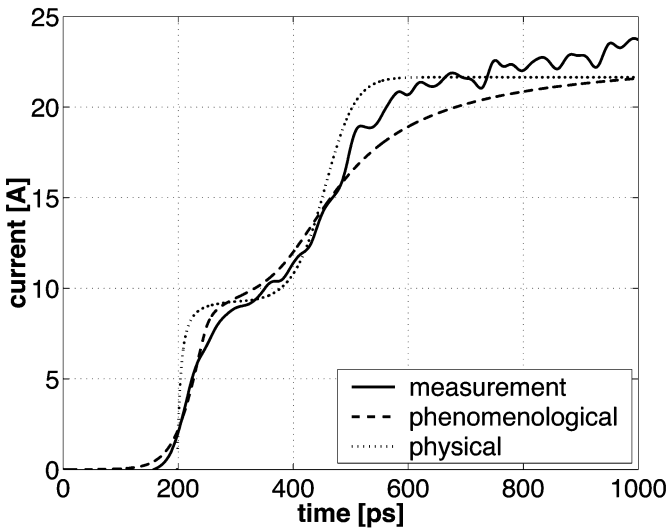

Fig. 16. Measurement and simulation of short-gap ESD arc current (electrode material steel, breakdown voltage 2300 V, gap distance 60 μm, $a_{\mathrm{M}} = 9 * 10^{-4}$ Vs/m, $a_T = 1.3 * 10^{-3}$ Vs/m, $E_T = 25$ kV/mm, and $\mathrm{K}(\alpha) = 0.4$).

TABLE III
MODEL CONSTANTS USED FOR ARC CURRENT SIMULATION AT DIFFERENT ELECTRODE MATERIALS

Electrode material	Aluminum	Brass	Steel
a_M (Vs/m)	$4*10^{-4}$	$4*10^{-4}$	$9*10^{-4}$
a_T (Vs/m)	$8*10^{-4}$	$8*10^{-4}$	$1.3*10^{-3}$
E_T (kV/mm)	32	12	25
A (Torr/m)	$1.33*10^{2}$	$2*10^{2}$	$1.1*10^{2}$
B (V*Torr/m)	$3.4*10^{4}$	$3.4*10^{4}$	$3.3*10^{4}$
K(α)	0.2	0.45	0.4

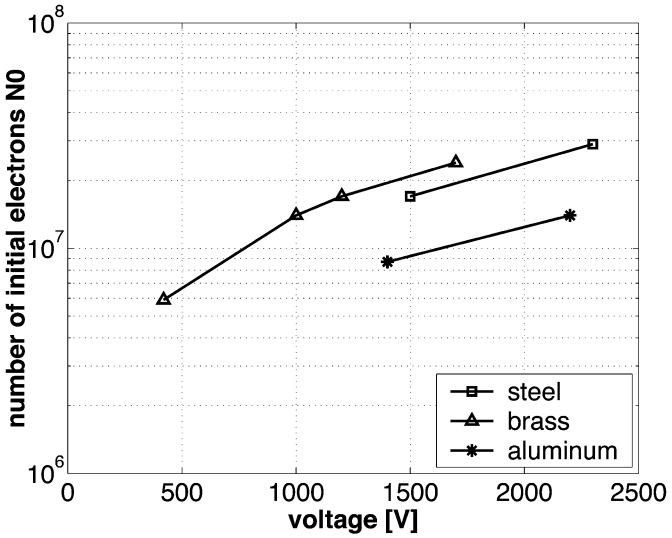

Fig. 17. Number of initial electrons supplied by the surface process at different electrode materials.

the resistive heating process and leading to reduced particle emission (i.e., reduced number of initial electrons N_0). The avalanche process simulated by the physical model ("Extended Toepler Law") develops too fast for some electrode materials (Fig. 15). The reason for that behavior however is unclear. A further fit of the ionization coefficient α may be needed. To attain a more consistent behavior, the movement, size and shielding properties of the space charge of the plasma front need to be considered in a more sophisticated way. It may be done by simulation on particle level [30], however, the lack of sufficient computing power stops us for now.

The charge carrier emission increases slightly by voltage (Fig. 17). Assuming mainly resistive heating of the electrode surface due to field emission current [6], the increasing voltage supplies more energy into the electrode surface leading to faster and/or deeper heating and explosive emission of more charge carriers into the gap.

V. CONCLUSION

Two models have been proposed for short-gap ESD modeling, a phenomenological model and a more complicated physical model. Both models are able to fit measured data on short-gap ESD in a reasonable manner. However the simple, phenomenological model seems to be better suited for the modeling of short-gap ESD. The models of the surface process and the avalanche process have been combined to facilitate a consistent time dependent behavior of the electrical parameters of an arc discharge in air.

An explosive charge carrier emission from electrode surface protrusions dominates the initial phase of the discharge. In the first approach, a model having a mathematical structure similar to an avalanche model is used for describing the surface process. The second approach to simulate the surface process has been derived from pulsed vacuum discharge modeling. However, the first approach gives better results.

The avalanche process has been simulated using the "Toepler Law" and the "Extended Toepler Law." The "Extended Toepler Law," using an initial number of charge carriers supplied by the surface process and known values for the ionization coefficient α is not able to fit the measured data on short-gap ESD. Values for α, able to fit measured data in an avalanche simulation on short-gap ESD at different electrode materials have been provided.

REFERENCES

[1] S. Bönisch, D. Pommerenke, and W. Kalkner, "Broadband measurement of ESD risetimes to distinguish between different discharge mechanisms," *J. Electrostat.*, vol. 56, no. 3, pp. 363–383, 2002.

[2] S. Bönisch and W. Kalkner, "Einfluß von Annäherungsgeschwindigkeit, Elektrodenmaterial und Luftfeuchtigkeit auf elektrostatische Entladungen (ESD) bei kleinen Abständen und Spannungen," in *Proc. EMV 2002—Int. Fachmesse und Kongreß für Elektromagnetische Verträglichkeit*, Düsseldorf, Germany, 2002, pp. 101–108.

[3] ——, "Influence of the approach speed, charge voltage and electrode material on the intensity and reproducibility of short gap electrostatic discharges," in *Proc. 15th Int. Zurich Symp. EMC*, Zurich, Switzerland, 2003, pp. 677–682.

[4] D. Pommerenke, "Transiente felder der elektrostatischen entladung (ESD)," Ph.D. dissertation, VDI Verlag, Technical University of Berlin, Berlin, Germany, 1995.

[5] A. Küchler, *Hochspannungstechnik*. Düsseldorf, Germany: VDI-Verlag, 1996.

[6] W. W. Dolan, W. P. Dyke, and J. K. Trolan, "The field emission initiated vacuum arc. II. The resistively heated emitter," *Phys. Rev.*, vol. 91, no. 5, pp. 1054–1057, 1953.

[7] J. Paulini, T. Klein, and G. Simon, "Thermo-field emission and the Nottingham effect," *J. Phys. D, Appl. Phys.*, vol. 26, no. 8, pp. 1310–1315, 1993.

[8] W. B. Nottingham, "Thermoionic emission from thungsten and thoriated tungsten filaments," *Phys. Rev.*, vol. 49, p. 78, 1936.
[9] ——, "Remarks on energy losses attending thermoionic emission of electrons from metals," *Phys. Rev.*, vol. 59, p. 906, 1941.
[10] ——, *Handbuch der Physik, Elektronen-Emission Gasentladungen I, Band 21*. Berlin, Germany: Springer-Verlag, 1956, pp. 1–175.
[11] P. H. Cutler, M. S. Chung, N. M. Miskovsky, T. E. Sullivan, and B. L. Weiss, "A new model for the replacement process in electron emission at high fields and temperatures," *Appl. Surf. Sci.*, vol. 76/77, pp. 1–6, 1994.
[12] F. M. Charbonnier, R. W. Strayer, L. W. Swanson, and E. E. Martin, "Nottingham effect in field and T-F emission: Heating and cooling domains, and inversion temperature," *Phys. Rev. Lett.*, vol. 13, pp. 397–401, 1964.
[13] G. M. Fleming and J. E. Henderson, "The energy losses attending field current and thermoionic emission of electrons from metals," *Phys. Rev.*, vol. 58, pp. 887–894, 1940.
[14] R. H. Fowler and L. Nordheim, "Electron emission in intense electric fields," in *Proc. Roy. Soc. A*, vol. 119, 1928, p. 173.
[15] P. A. Chatterton, "A theroretical study of field emission initiated vacuum breakdown," in *Proc. Phys. Soc.*, vol. 88, 1966, pp. 231–245.
[16] M. Toepler, "Zur Kenntnis der Gesetze der Gleitfunkenbildung," *Analen der Physik, 4. Folge, Band 21*, pp. 193–222, 1906.
[17] ——, "Zur Bestimmung der Funkenkonstanten," *Archiv für Elektrotechnik*, 1927.
[18] K. Möller, "Ein Beitrag zur experimentellen Überprüfung der Funkengesetze von Toepler, Rompe-Weizel und Braginskii," *ETZ A, Band 92, Heft 1*, 1971.
[19] W. Weizel and R. Rompe, "Theorie des elektrischen Funkens," *Ar. Physik, Leipzig, 6. Folge, Bd. 1*, pp. 285–300, 1947.
[20] F. Paschen, "On sparking over in air, hydrogen, carbon dioxide under the potentials corresponding to various pressures," *Wiedemann Annalen der Physik und Chemie*, pp. 69–96, 1889.
[21] J. Townsend, *Electricity in Gases*. London, U.K.: Oxford Univ. Press, 1914.
[22] S. I. Braginskii, "Theory of the development of a spark channel," *Sov. Phys. JETP, Bd. 7*, pp. 1068–1074, 1958.
[23] J. M. Meek and J. D. Craggs, *Electrical Breakdown of Gases*. New York: Wiley, 1978.
[24] I. I. Levintov, (in Russian)*DAN SSSR*, vol. 85, no. N6, pp. 1247–1250, 1952.
[25] I. N. Slivkov, V. I. Mikhailov, N. I. Sidorov, and A. I. Nastukha, "Electrical breakdown and discharge in vacuum" (in Russian), *Atomizdat*, p. 300, 1966.
[26] G. A. Mesyats and D. I. Proskurovsky, *Pulsed Electrical Discharge in Vacuum*. Berlin, Germany: Springer-Verlag, 1989.
[27] ——, "Current growth in pulse breakdown of a short vacuum gap," *Izv. Vyssh. Uchebn. Zaved. Fiz. 1*, pp. 81–85, 1968.
[28] Y. D. Korolev and G. A. Mesyats, *Physics of pulse breakdown in gases*. Yekateringburg, Russia: URO-Press, 1998.
[29] G. E. Georghiou, R. Morrow, and A. C. Metaxas, "The theory of short-gap breakdown of needle point-plane gaps in air using finite-difference and finite-element methods," *J. Phys. D, Appl. Phys.*, vol. 32, no. 12, pp. 1370–1385, 1999.
[30] J. P. Verboncoeur, A. B. Langdon, and N. T. Gladd, "An object-oriented electromagnetic PIC code," *Comp. Phys. Comm., 87*, pp. 199–211, May 11, 1995.
[31] S. Nitta, A. Mutoh, and K. Miyajima, "Generation mechanism of showering noise waveforms—Effect of contact surface variations and moving velocity of contact," *IEICE Trans. Commun.*, vol. E79-B, no. 4, pp. 468–473, 1996.

Sven Bönisch was born in Berlin, Germany, in 1971. He received the Dipl.-Ing. degree in electrical engineering from the Technical University of Berlin, Berlin, in 1998. He is currently working toward the Ph.D. degree at the Department of High Voltage Engineering, the Institute of Energy and Automation Technology, Berlin, where he is involved in the investigation of short-gap ESD at low voltages and the development of partial discharge measurement techniques on high voltage cables.

He worked for two years in high frequency, analog and digital circuit design and then became a Scientific Research Assistant at the Department of High Voltage Engineering, the Institute of Energy and Automation Technology.

Wilfried Kalkner was born in 1942. He received the Dipl.-Ing. and Dr.-Ing. degrees in electrical engineering from the Technical University of Berlin, Berlin, Germany, in 1969 and 1974, respectively.

He worked for about ten years in the cable industry, mainly in research and development of extruded insulation cables and accessories. Since 1977, he has lectured in electrical insulation techniques at the Technical University of Berlin. Since 1984, he has been a full Professor of high-voltage engineering.

David Pommerenke (M'98) was born on April 11, 1962, in Ann Arbor. MI. He received the electrical engineering and Ph.D. degrees on transient fields of ESD from the Technical University Berlin, Berlin, Germany, in 1989 and 1995, respectively.

In 1989, he became a Research and Teaching Assistant in EMC and High Voltage with the Technical University of Berlin. In 1996, he joined Hewlett-Packard. He accepted a faculty position at the Electromagnetic Compatibility Group, University Missouri-Rolla, in 2001. His reserach interests include electrostatic discharge, partial discharge in high-voltage systems, electronics, measurement instrumentation design, and electromagnetic compatibility.